

Experimental Investigation of Solid Rod Cathode Operation*

J. E. Polk[†], K. D. Goodfellow[‡], T.J. Pivirotto[†]

Jet Propulsion Laboratory
California Institute of Technology
Pasadena, California

Abstract

A series of models have been CIC.VC1OIM1 to describe the temperature distribution of thermionic cathodes in high current discharges in an effort to evaluate cathode service life. A number of experimental measurements have been made to validate these models and provide values of the input parameters. A database of axial temperature distributions on a cylindrical, 2 percent thoriated tungsten cathode has been collected for current levels ranging from 600 to 1000 A at an argon mass flow rate of 0.75 g/s and ambient gas pressures ranging from 1500 to 6000 Pa. Additional measurements indicate a surface emittance of about 0.6. The variation of the attachment area with current and pressure was characterized by measuring the intensity distribution of an argon ion line near the cathode surface. Pressure measurements made at the tip of the cathode show a consistently lower tip pressure than the tank pressure measured on the chamber door. Examination of the surfaces of several cathodes after varying lengths of operation shows the evolution of surface microstructure and reveals the preferential deposition of thorium metal on the cathode tip.

Introduction

The service life of thermionic cathodes is important for a number of high current discharge devices, particularly several classes of electric thrusters such as electrothermal arcjets and magnetoplasmadynamic (MPD) engines. Low thrust levels dictate burn times of several thousand hours, and the cathodes of these devices are often the life-limiting component. High-current cathodes are subject to failure modes which can be classified as either event-consequent or the result of damage accumulation. Event-consequential failures, such as cathode melting as a result of excessive resistive heating, are the result of a single catastrophic event and can be adequately characterized by testing alone. However, it is impractical to characterize the failure risk associated with damage accumulation failure modes by testing alone because of the extremely long test durations required to observe

*Copyright © 1991 American Institute of Aeronautics and Astronautics, Inc., with permission.

[†]Technical Group Leader, Advanced Propulsion Technology Group

[‡]Member of the Technical Staff, Advanced Propulsion Technology Group

the failures. Validation of cathode service life under conditions where damage accumulation failure modes are critical therefore must rely heavily on modeling of the physics of failure. The role of testing is to identify the critical failure modes, validate the models of failure and provide information on the model input parameters such as material properties and operating environment.

High current cathodes are being studied at the Jet Propulsion Laboratory as a part of the Advanced Propulsion Concepts program. The goal of the program is to develop long-lived cathodes and the analytical tools to validate their service life. Cathode erosion, which appears to be the dominant damage accumulation failure mode, has been shown to depend strongly on the cathode temperature [1]. Therefore, part of this study is intended to provide a simple means of predicting the cathode temperature for various thruster operating conditions. In addition, the thermal characteristics of the electrodes must be known to compute the overall thruster thermal loads to the spacecraft. Models must also provide the appropriate boundary conditions at the cathode surface for models of the operating characteristics of the thruster. For example, the current contours within the magnetoplasmadynamic thruster cannot be specified independently of the cathode temperature distribution because the majority of the current is from thermionic emission. Since the cathode model boundary conditions also depend on the characteristics of the main plasma, the two models must be ultimately coupled to obtain an overall model of the cathode region of the thruster.

A series of models describing the cathode and plasma interaction are being developed. The cathode model consists of two parts, namely a near-cathode plasma model and a thermal model of the cathode[2]. The near-cathode plasma model connects the properties of the main plasma with the cathode. Specifically, given the plasma properties within a mean-free-path of the surface, the near-cathode model predicts the heat flux and current density to the cathode surface. With these boundary conditions and the traditional thermal transport mechanisms, the thermal model can predict the temperature distribution within the cathode. Because of the interdependency of the two models, they must be solved simultaneously. The input parameters used by the model for the plasma consist of the sheath voltage, the electron temperature, the pressure, the ionization energy of the gas, the ion mass, the surface work function, and the surface temperature. The arc attachment area is also specified to limit the total current, which is calculated using the given attachment area and the calculated current density distribution. The thermal model inputs consist of the base temperature or heat flux, the convection coefficient and environmental temperature, the surface emittance and environmental temperature, and the material thermal conductivity and resistivity. A series of thermal models have been developed with different levels of approximation. The nonlinearities of the system equations can present numerical difficulties. The simpler, one-dimensional models can be used to provide starting points for the more complete two-dimensional models, significantly reducing the computational time required. Although the quasi-two-dimensional models provide a good first approximation, a two-dimensional model is required for a detailed understanding of the processes involved.

The focus of the experimental part of the program is to test new cathode concepts, identify the critical failure mechanisms, provide a database of measurements to validate the cathode models and determine the values of the critical model drivers such as work function and gas pressure. The purpose of this paper is to present a database of temperature profiles recently obtained over a range of ambient pressures and current levels for cylindrical, 2 percent thoriated tungsten cathodes.

Comparisons of the model with preliminary thermal data showed good agreement at currents below about 1000 A and pressure levels greater than 1500 Pa [3], so these experiments concentrated on this parameter range. In addition, the cathode surface emittance, the size of the attachment area, the pressure on the cathode tip and the distribution of thorium, which determines the work function, were characterized to provide inputs to subsequent modeling efforts.

Experimental Apparatus

The Cathode Test Facility

The cathode test facility is shown in the diagram in Fig. (1). The stainless steel vacuum chamber is 0.5 m in diameter and 2.4 m long and is composed of 4 water-cooled cylindrical segments.

In addition, a water-cooled copper liner has been inserted in the middle two segments to permit long-duration operation. As the schematic in Fig. (2) shows, the first segment forms the discharge chamber. A water-cooled, ring-shaped copper anode with a diameter of 7.6 cm is mounted on a flange located between and electrically isolated from the first two tank segments. The cathode fixture mounted on the vacuum chamber door is composed of two coaxial tubes electrically isolated from each other and the door with micarta rings. The inner tube serves as the cathode current feed and has a water-cooled cap on the end to which the cathode is clamped. The outer tube is electrically floating and has a water-cooled copper disk mounted on the end with an aperture through which the cathode protrudes. The propellant gas is injected between the two tubes and flows into the discharge chamber through an annulus around the base of the cathode. The interelectrode gap is set by the thickness of a spatter in the cathode assembly. The cathodes used in this investigation were rods of 2 percent thoriated tungsten 76111111 long and 9.5 mm in diameter with hemispherical tips. The last tank segment contains a heat exchanger made of water-cooled, finned copper tubing to cool the exhaust before it enters the pumping system. The tank has a number of ports which provide optical access to the discharge chamber as well as the plume. In addition, the cathode and the discharge can be viewed along the tank axis through a window at the rear of the tank.

The vacuum chamber is pumped by a 610 l/s Roots blower backed by a 140 l/s Stokes mechanical pump. The system is capable of achieving a vacuum of less than 0.13 Pa with no propellant flow and approximately 80 Pa with an argon flow rate of 0.75 g/s. Higher ambient gas pressures are achieved by throttling the pumping speed with a valve on a bypass around the main vacuum valve. The ambient pressure can be controlled to within approximately ± 30 70 Pa. The arc is powered by two Miller welding power supplies, each of which can provide 1500 A at a load voltage of 40 V continuously or 2000 A at 40 V with a 50 percent duty cycle. The initial arc breakdown is accomplished with a 4 A, 850 V start supply.

Diagnostics

The factory shunts in the Miller welders have been replaced with precision shunts that are used to monitor the arc current. The terminal voltage is measured at the current feedthroughs into the tank. The propellant flow rate is measured with a Sierra Instruments Side-Trak Model 830 flow meter and a Micromotion Model D6 flow meter and controlled with a throttling valve located just

Figure 1: Diagram of the cathode test facility.

Figure 2: Schematic of the electrode configuration.

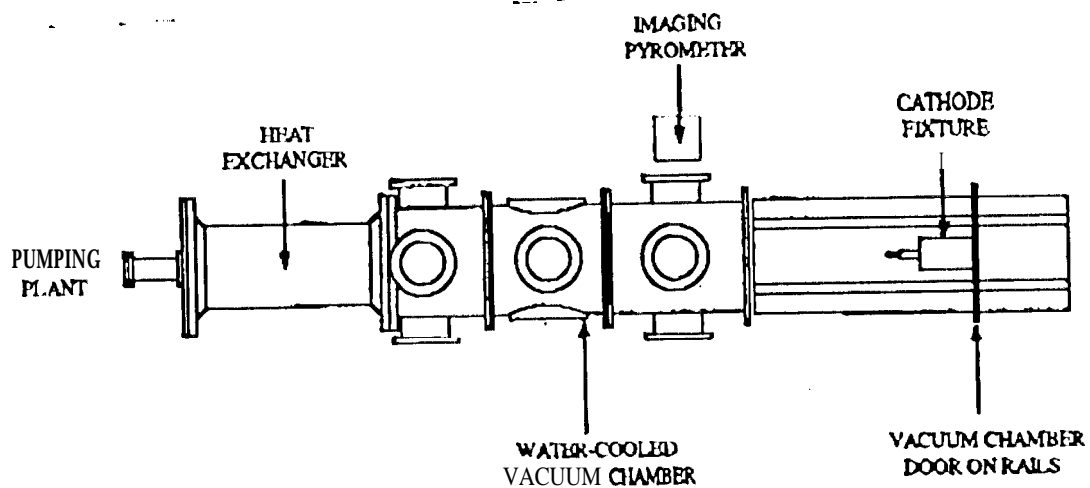


Figure 1: Diagram of the cathode test facility.

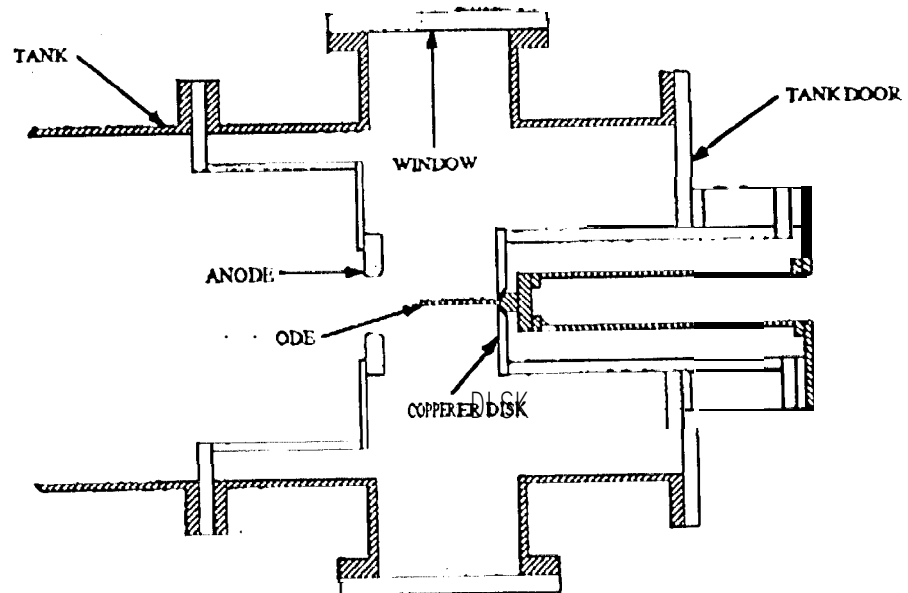


Figure 2: Schematic of the electrode configuration.

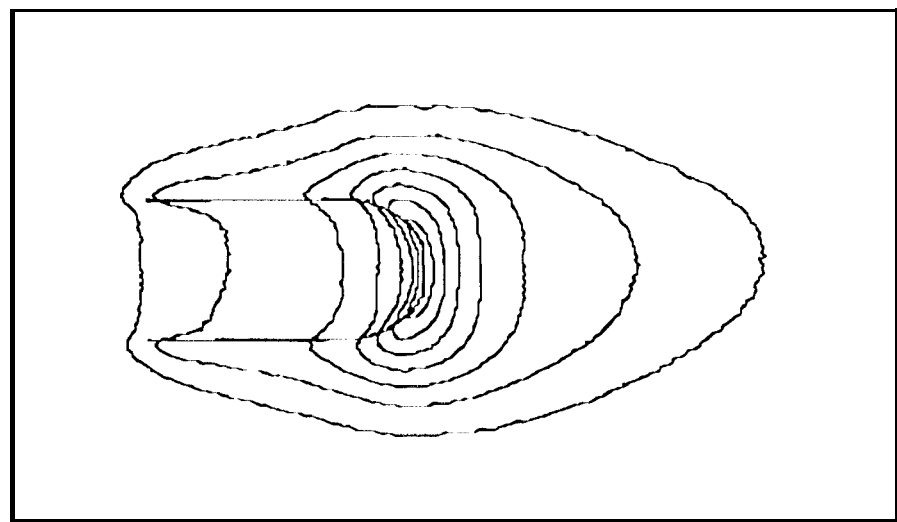
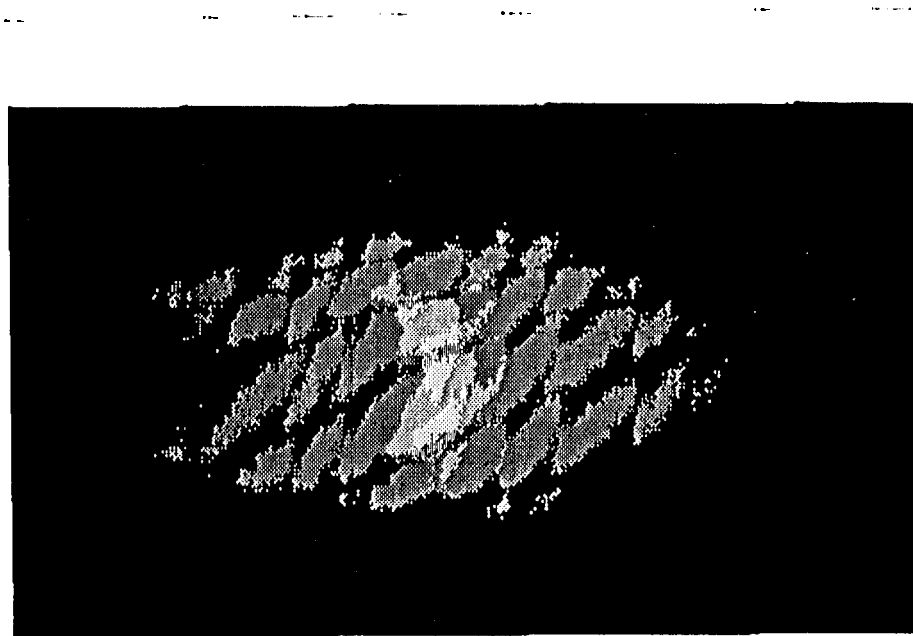


Figure 11: Distribution of the 488 nm Ar II line intensity distribution at 800 Å and 1500 Pa.

upstream of the inlet to the cathode fixture. The flow meter output was calibrated by measuring the mass loss from an argon bottle as a function of time. Three MKS Barotron capacitance manometers with ranges of 0 133 l's, 0 1.3×10^4 Pa, and 0 1.3×10^5 Pa are used to monitor pressures. The three transducers are mounted in a single manifold with two input tubes. One line measures the tank pressure through a feedthrough 011 the chamber door. A special cathode was fabricated with a 1 mm diameter hole bored the entire length along the centerline, which serves as a pressure tap to measure the pressure at the cathode tip. This pressure tap was connected to the other manifold inlet. Either pressure could be read independently by valving off the other input. These parameters and a number of facility temperatures are recorded with a Macintosh computer system utilizing LabView software and National Instruments multi-function I/O cards.

A CHDTEC 2250-1D Charge Injection Device (CID) camera was chosen as an optical pyrometric sensor to measure the two-dimensional temperature field on the cathode. The system optics are composed of two interference filters with a 10 nm bandpass centered at 632.8 nm and a long pass filter with a cutoff wavelength of 570 nm. The camera lens aperture is fixed at a relatively small value of f/4 and neutral density filters are used to control the image intensity. The imaging array has 512 x 512 CID detectors which are read out at a maximum rate of thirty times per second. These values are converted to an analog signal, which is then further processed and output as a normal video signal by the camera electronics. The video signal is digitized by a Data Translation DT-2862 8-bit frame-grabber board, which yields a final value between 0 and 255 corresponding to the incident power. The camera output was calibrated as a function of incident radiance using a tungsten ribbon lamp. The calibration procedure and a detailed error analysis for the temperature measurements are discussed in [4].

In the experiments the camera and optics were mounted outside the chamber about 39.5 cm from the cathode. The video output from the camera was digitized to provide real-time monitoring of the temperature distribution. One line in video memory chosen to correspond to the axis of the cathode was sampled from each frame. A given number of lines were averaged, displayed in real time, and periodically stored on disk.

The surface emittance was measured using a special cathode fabricated with radial cavities located at axial locations 4.5, 10 and 15 mm from the cathode tip. The 1 mm diameter, 4 mm deep cavities were formed by electrodischarge machining. Experiments and theoretical calculations yield an emittance of about 0.95 for cavities with this length-to-diameter ratio and rough walls [5,6]. The emittance of the surrounding cathode surface was calculated by comparing the radiance of the cavities with the surface radiance.

The camera was also used to study the extent of the arc attachment region. Two interference filters with a 10 nm bandpass centered at 488 nm were used to select radiation from an intense argon ion line. Entire images of the cathode and near-cathode discharge region were then captured with the frame grabber board and analyzed to yield the lateral intensity distribution. These measurements were used to calculate an upper bound on the arc attachment area and the average current density in the attachment zone.

Emission spectroscopy was also used to resolve certain features of the bright plasma near the cathode surface. An image of the cathode was formed 011 a screen with a lens mounted outside the vacuum chamber. A length of fiber optic cable was installed with the 100 micron diameter inlet

located at the center of these rccm and flush with the image plane. The screen and fiber inlet were mounted on a micrometer-operated X-Y translation stage so that the inlet could be positioned at any desired point in the image. With this technique, light-gathering with high spatial resolution from any image point could be achieved. The light emerging from the fiber exit was focused on the entrance slit of a one-meter McPherson monochromator using an optical system designed to match the fiber numerical aperture with that of the monochromator. Variable monochromator slits were set at 30 to 50 microns and a 1200 groove per mm grating was used to disperse the light, providing a potential resolution in first order of 0.10 Angstroms. The output of a Hamamatsu R928 photomultiplier tube was displayed on a strip chart recorder.

The surface microstructure and elemental composition of cathodes after operation for various lengths of time were analyzed using a scanning electron microscope (SEM) and energy-dispersive spectroscopy (EDS). These measurements were used to characterize changes in the surface finish and the distribution of thorium metal on the surface.

Experimental Results

Cathode Surface Emittance

Knowledge of the emittance is not only of importance in predicting the radiant heat flux as a boundary condition on the thermal models, it is also required to convert the radiance measured directly by the imaging pyrometer to surface temperatures. The cathode with the three cavities was imaged in a series of experiments at 1000 A with tank pressures of 1500 to **3000** Pa and argon mass flow rates of 0.25 to 0.75 g/s. The radiance from the back walls of the cavities and from spots on the cathode surfaces in the same axial locations and approximately 1 mm from the centerline of the cylindrical cavities was measured. The surface emittance calculated from the ratio of the radiances and a cavity emittance of 0.95 is shown in Fig. (3). The emittance is essentially uniform along this part of the cathode and ranges from 0.53 to 0.66. This is higher than emittances measured by de Vos on polished tungsten ribbons [7] and in similar experiments by Myers [8] in a low power MIJ thruster, but agrees well with later measurements by Fillmore on a similar thruster [6]. Subsequent elemental analysis of the area surrounding the cavities using Energy Dispersive Spectroscopy (EDS) showed only pure tungsten, but Scanning Electron Microscope (SEM) examinations revealed a very complex microstructure. The observed increase in emittance is consistent with measurements for tungsten with a characteristic surface roughness of 1-3 microns [9].

When plotted as a function of the local temperature in Fig. (4), the measurements indicate a slight decrease in emittance with increasing temperature. This behavior was also observed by de Vos [7] and Fillmore [6]. A mean value of about 0.57 was chosen for all subsequent thermal data analysis.

Axial Temperature Distributions

The focus of this experiment is the development of a database of temperature measurements for use in validating the models. The axial temperature distribution in the first 15 to **40** mm of the cathode (measured from the tip) was determined using the imaging pyrometer for current levels of

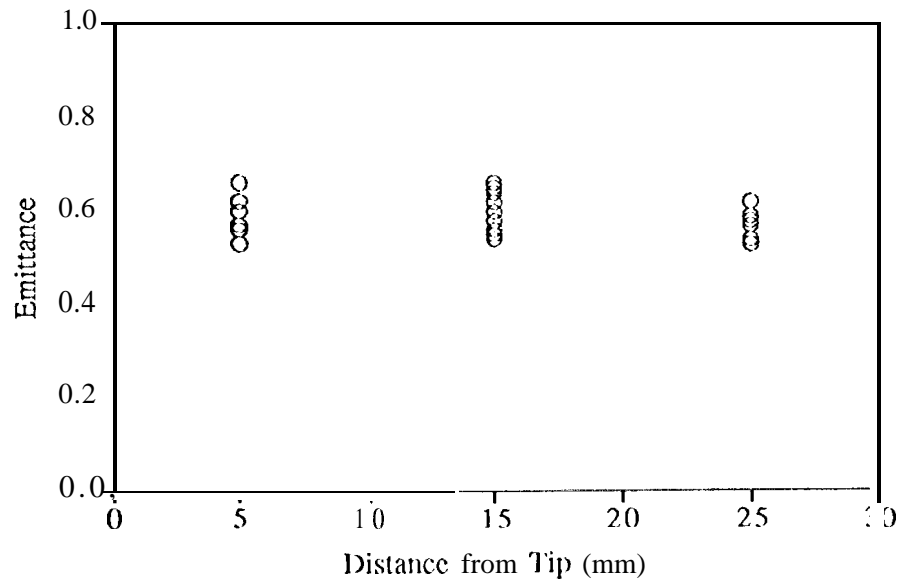


Figure 3: Cathode surface emittance measured at three axial locations.

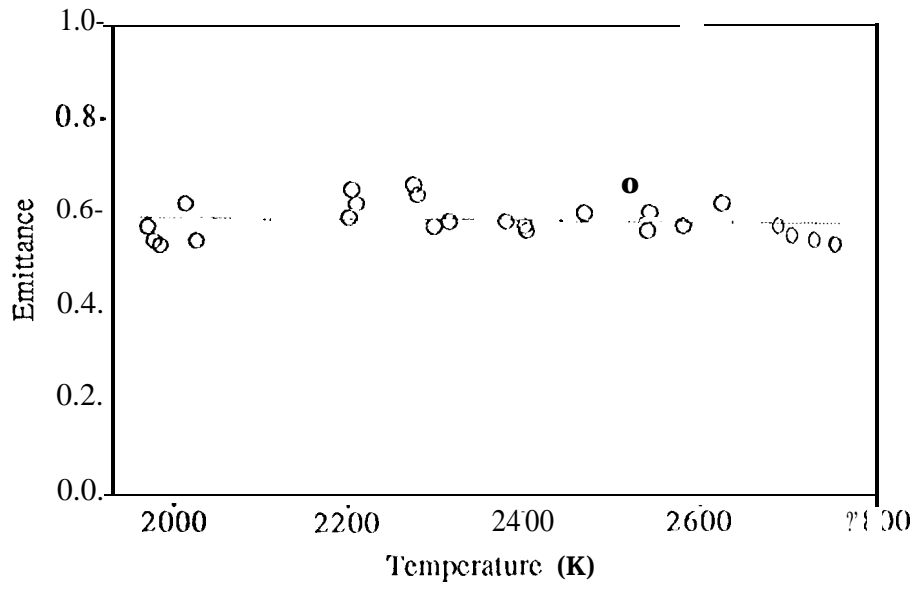


Figure 4: Cathode surface emittance as a function of surface temperature.

600, 800" and 1000 A, tank pressures of 1500, 3000, 4500 and 6000 Pa and an argon mass flow rate of 0.75 g/S. Typical results are shown in Figures (5) (8).

At the tip, the temperature increases weakly with current for all pressures. However, a more dramatic increase in temperature with current is observed on the cathode shaft. The location of the attachment zone edge was estimated by filter photography (described in detail in the next section) and plotted on the temperature profiles. In all cases the behavior of the temperature profile upstream of the attachment zone edge is very regular, reflecting thermal transport dominated only by conduction, radiation and convection. Inside the attachment zone, where the more complicated arc heating mechanisms dominate, the profiles are more complex. A qualitatively different temperature distribution occurs for the lowest pressure, as first observed in [4]. At lower pressures a temperature peak is located on the shaft of the cathode, while at higher pressures the peak is located on the tip. Many of the temperature profiles at higher pressure also show a change in slope inside the attachment zone. The intensity peak at the tip may contain some contribution from plasma radiation, either the continuum in the 10 nm bandpass of the 632 nm interference filter or the integrated effect of plasma radiation collected in the wings of the blocking filters. However, measurements of the plasma intensity off of the cathode surface indicate that this contribution is small. In addition, the timescale for decay of the tip intensity peak when the arc is extinguished is much longer than the plasma decay timescales, proving that the peak is due to surface luminosity.

The variation of the peak temperatures with current and pressure is summarized in Fig. (9). This figure shows the weak dependence of peak temperature on current and the much stronger effect of tank pressure.

The profiles in Fig. (6) demonstrate the degree of irreproducibility in the cathode temperature for the same operating point. While the tip temperature is generally quite repeatable, temperatures on the shaft can vary by as much as 100 K from one trial to the next. The shapes of the curves are all very similar, but in some cases they are displaced upward by the appearance of a temperature peak or plateau upstream of the tip. This suggests that additional heating is occurring in this location which pulls the distribution to higher temperatures. Some of the irreproducibility can be attributed to varying run durations, because the temperature distribution appears to evolve with time. The evolution of the temperature profile during a five hour run at 1000 A, 3000 Pa and 0.75 g/s is summarized in Fig. (10), which displays the tip temperature calculated assuming an emittance of 0.57 and the temperature at each of the three cavities calculated with an emittance of 0.95. The dotted lines are interpolated values in regions where the tip temperature and cavity temperatures were not available because the measurement line was moved off of the axis to monitor the radiance outside the cavities. The discontinuous increase in the temperatures at about 10 minutes elapsed time occurred when the current was increased from the start value of 800 A to the 1000 A operating point. After a transient lasting only several minutes, the tip temperature becomes relatively constant at 2750-2780 K. However, after about two hours the temperature on the shaft starts to climb. The high temperature zone is effectively creeping back on the cathode shaft. The fact that the cavity radiance shows this effect suggests that it is a true increase in temperature, not just an increase in emittance. These transients are most likely due to an increase in the length of the attachment zone precipitated by changing surface conditions, as discussed below.

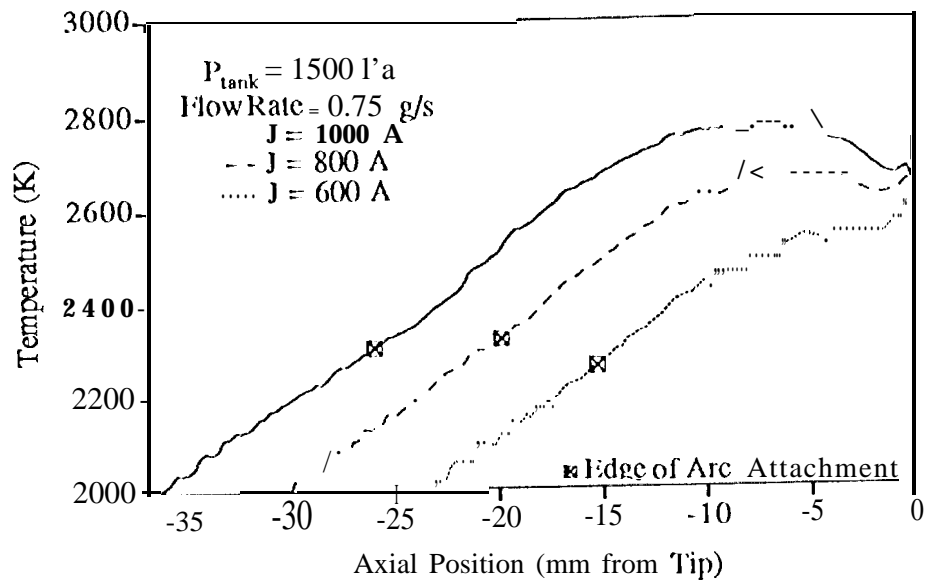


Figure 5: Axial temperature distribution for a tank pressure of 1500 Pa.

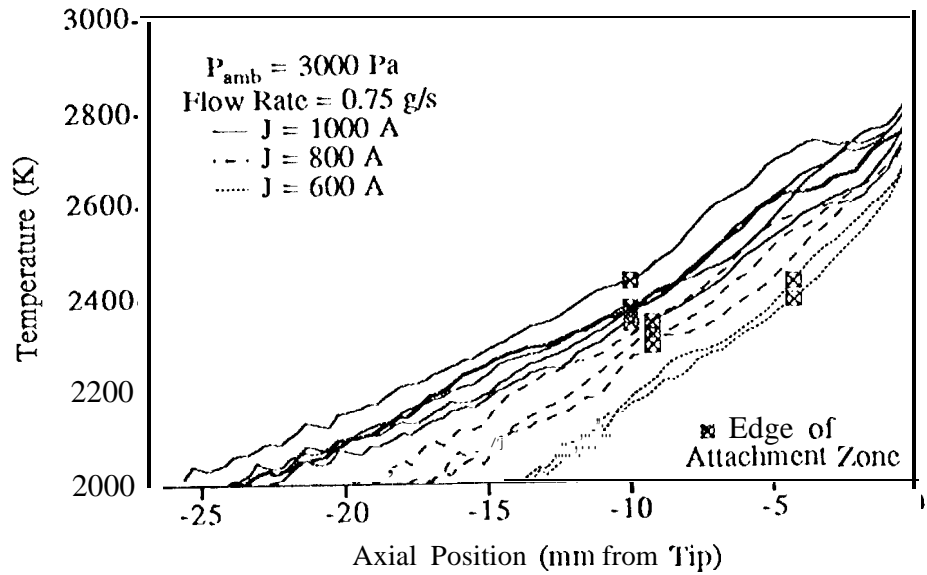


Figure 6: Axial temperature distribution for a tank pressure of 3000 Pa.

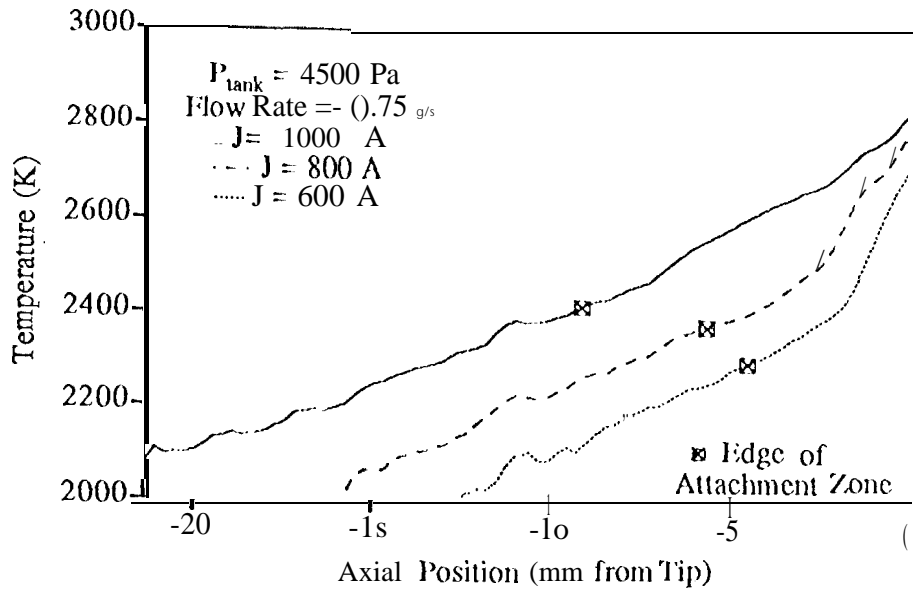


Figure 7: Axial temperature distribution for a tank pressure of 4500 Pa.

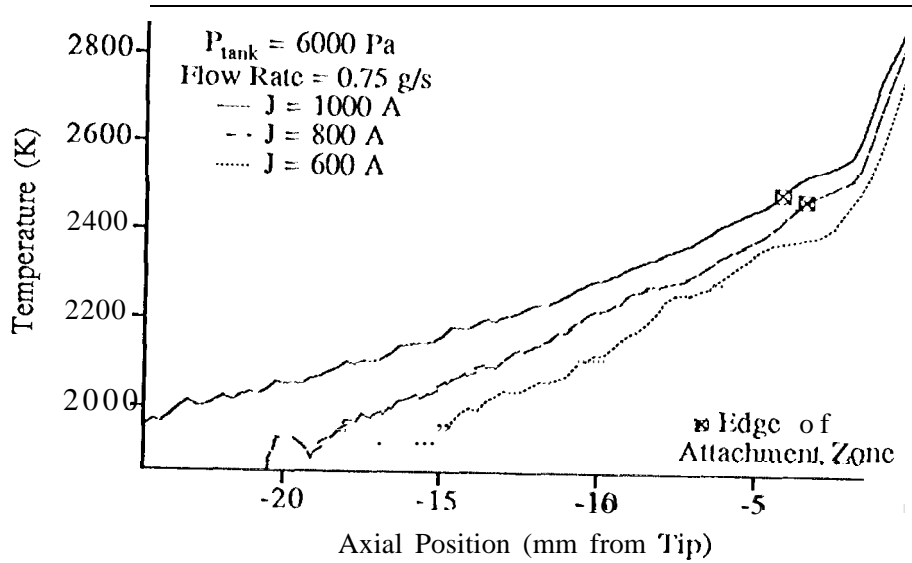


Figure 8: Axial temperature distribution for a tank pressure of 6000 Pa.

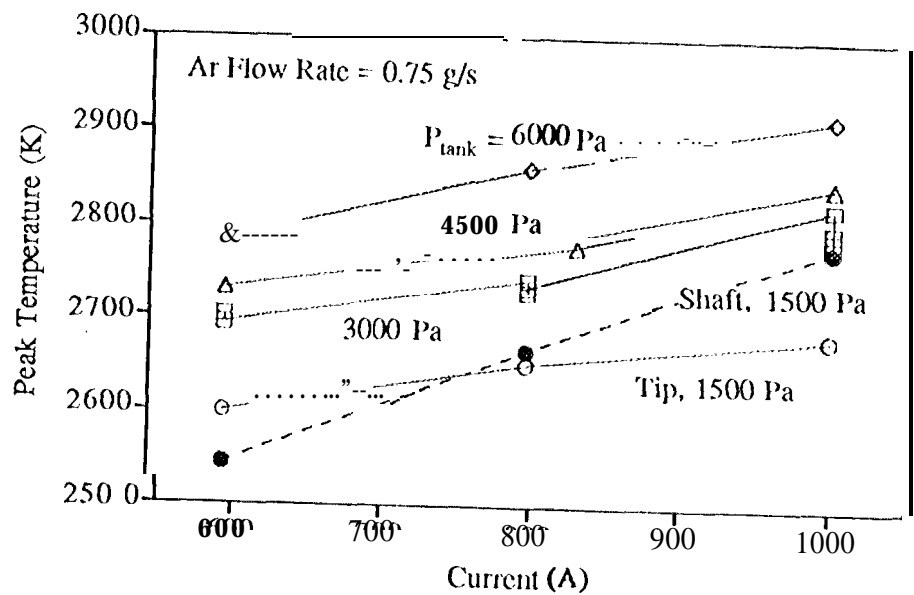


Figure 9: Variation of the peak temperatures with current and pressure.

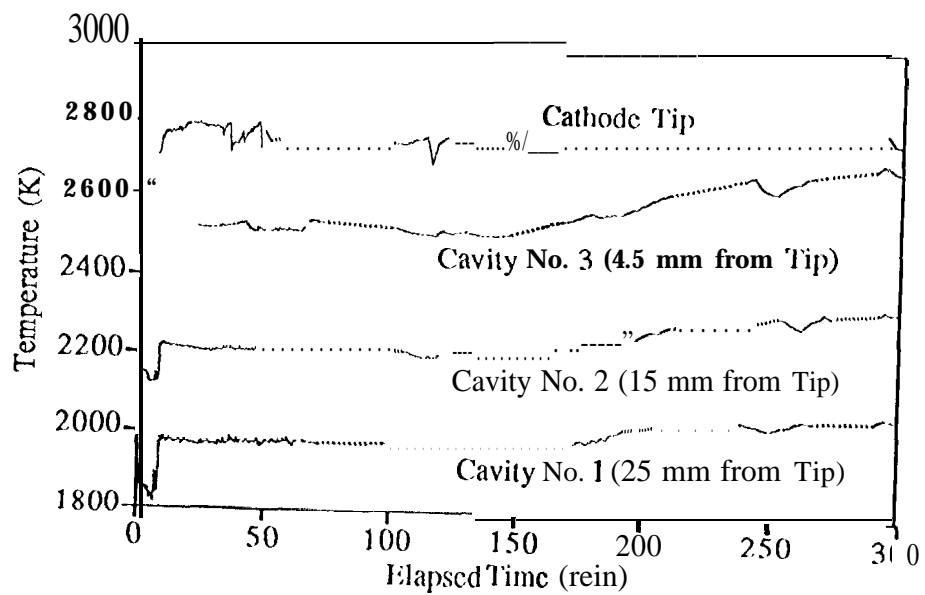


Figure 10: Variation in cathode temperature with operating time.

The Arc Attachment Area

The extent of the arc attachment zone is an important parameter in the model because it determines what fraction of the boundary is subjected to the arc heat inputs and is used computationally to limit the total current to the desired value. It is, of course, very difficult to measure directly the surface current density or the heat fluxes. In these experiments the arc attachment region was identified by using filter photography and emission spectroscopy to resolve the regions of most intense argon ion line emission. This approach should give an estimate of the attachment on the cathode surface. A typical image of the cathode and discharge region captured with the CII camera using two 488 nm interference filters is shown in Fig. (11) with a contour plot of the 488 nm Ar II line intensity distribution. The contours represent lines of constant camera response in gray levels and start from 30 on the outside, increasing inward in increments of 30.

This example shows the common features of the arc attachment zone. There is a strong axial gradient in intensity downstream of the cathode which is probably due to a decrease in current density as the current lines diverge toward the anode, and a drop in density and temperature as the flow accelerates. There is also a strong radial gradient that reflects a true increase in density due to magnetic pinching and an increase in integrated lateral luminosity due to a lengthening optical path length through the cylindrical plasma column. To transform the lateral intensity distributions to true radial intensity profiles requires the use of an inversion technique. The capability to invert image data using an Abel transform to resolve these two possible effects is now being implemented, but the results were not yet available for this paper. All of the profiles show a strong peak in intensity along the hemispherical tip of the cathode. Two experiments were performed to verify that this peak is not due to cathode surface luminosity. First, the intensity in this region was monitored during arc extinction, which revealed a decay transient lasting less than 1/30 of a second, the minimum temporal resolution of the camera system. Second, a monochromator was used to gain finer spectral resolution of the intensity peak than the filter photography could provide. In axial scans from the cathode shaft into the plasma plume downstream of the cathode a strong peak in the intensity at 488 nm similar to that in the photographs was found, but no increase in luminosity was observed in the continuum near the 488 nm line. These two experiments confirm that the observed peak is due to intense argon ion line emission. The large radial extent of the intensity plateau at this axial location also suggests that it is not just due to the longer optical path along the center of the image. This bright plasma cloud on the tip of the cathode may be the ionization zone located above the sheath, marking the part of the attachment zone with the highest current density.

The intensity distributions measured at a number of different discharge currents and tank pressures are presented in Fig. (12). All of the contours presented here have been adjusted to the same relative intensity so that they can be compared. Comparison of the images reveals that the size of the attachment zone increases with current and decreases with tank pressure, as predicted by the models [3]. This behavior was also observed by Hügel [10]. The distributions for a pressure of 1500 Pa show much more plasma intensity along the cathode shaft, mirroring the behavior observed in the temperature measurements.

A quantitative estimate of the arc attachment axial length and area was obtained from these

Figure 11: Distribution of the 488 nm Ar I 11 line intensity distribution at 800 A and 1500 l'a.

Figure 12: Comparison of 48811111 Ar 11 line intensity distributions.

images by using the last contour line as the attachment zone edge. The axial length and enclosed area are plotted in Fig. (13) as **functions of current and pressure**.

These values in general are much larger than the attachment area calculated with the cathode models [2,3]. Using the entire plasma zone may therefore overestimate the heat input area which is required by the model. As suggested above, the extent of the bright region at the tip may be a more appropriate length scale for the arc heating area. A quantitative assessment will be attempted when true radial intensity profiles are available.

The upper bound on arc. attachment area was used to calculate the average current density. The results are plotted in Fig. (14) as a function of current and pressure. The values are relatively constant for a given pressure, reflecting a roughly linear relationship between attachment area and current, and range from about 100 A/cm^2 for 1500 Pa to 800 A/cm^2 for 6000 Pa . Because the temperature increases considerably downstream of the attachment zone edge, a highly nonuniform axial current density distribution is to be expected. These values of average current density will therefore underestimate the current density in the tip. In fact, the edge of the luminous plasma zone represents the point where the current density falls below a value which produces sufficient ionization to make the plasma visible at 488 nm . Comparison of the attachment lengths with the temperature profiles in Figures (5)(8) shows that this occurs at a cathode surface temperature ranging from about 2200 and 2400 K .

Cathode Tip Pressure Measurements

The cathode thermal models are quite sensitive to the pressure near the cathode surface because it plays an important role in determining the heat flux from the sheath region. The thermal models have been modified to self-consistently calculate the radial pressure gradient which is supported by a radial $j_z B_\phi$ force, where j_z is the axial current density and B_ϕ is the self-induced azimuthal magnetic field [3]. Assuming a uniform current density given by $I_{tot}/\pi r_c^2$, where I_{tot} is the total current, and integrating this force over an arc. column of radius r_c yields a pressure difference between the ambient pressure and the centerline pressure of

$$P_{amb} - P_{tip} \approx -\frac{\mu_0 I_{tot}^2}{8\pi^2 r_c^2} \quad (1)$$

where μ_0 is the permeability of vacuum. Estimates based on this relationship using the current levels and arc column radii from the experiments suggest that a pressure increase of several hundred Pa over the ambient pressure should be observed on the cathode tip. Such overpressures have been experimentally confirmed in a self-field device under similar operating conditions [11].

However, in these experiments the exact opposite behavior was observed. As shown in Fig.(15), the pressure measured with the pressure tap on the centerline of the cathode is substantially lower than the measured tank pressure. The pressure difference decreases slightly with increasing current and ranges from 1600 to 1800 Pa for a tank pressure of 3000 6000 Pa and is about 1100 Pa for a tank pressure of 1500 Pa .

A number of experiments were performed to test the validity of the pressure tap measurements. Because the same pressure transducer was used to measure both the tank pressure and the cathode

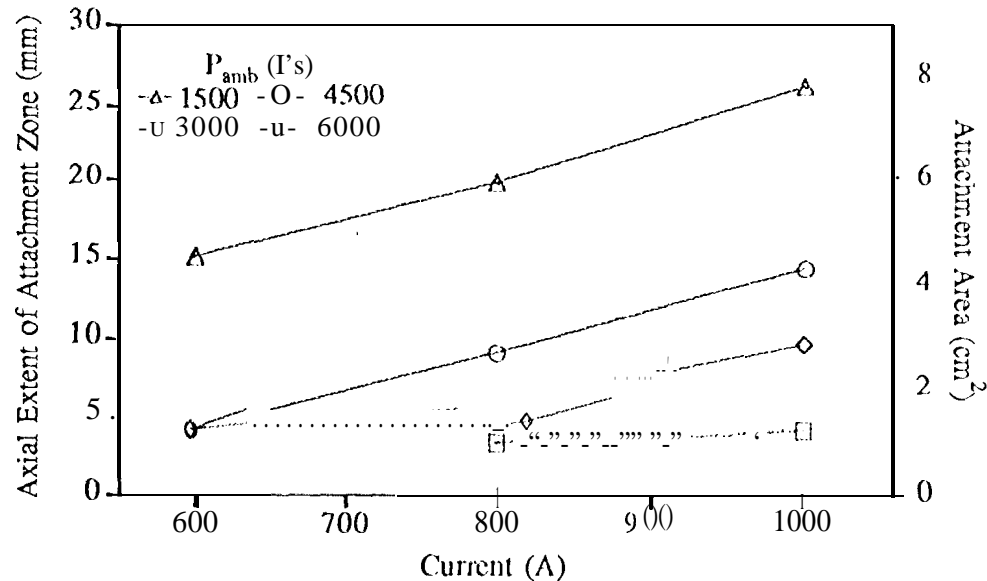


Figure 13: Estimates of the attachment zone axial length and enclosed area.

centerline pressure, sensor effects such as electrical noise from the arc can be ruled out. A return to the low centerline pressure reading after pressurizing and isolating the pressure tap line showed that the pressure tap in the cathode was not blocked during arc operation. As shown in Fig. (16), the pressure measured through the pressure tap recovers to the tank pressure level when the arc is extinguished and drops to the low value again when it is restarted. After two hours of operation the cathode pressure tap was examined and found to be undamaged. After a total of 1310111S a thin shell of tungsten was discovered over the orifice, but cracks in the shell apparently still provided sufficient communication to measure the pressure, but with a somewhat longer response time. The problem may lie in the assumption that the tank pressure measured on the chamber door approximately 40 cm from the cathode tip is representative of the ambient pressure near the cathode. To test this concept, a cathode with a second pressure tap located on the shaft upstream of the attachment area is being fabricated. This should provide a better measurement of the local ambient pressure.

Cathode Surface Microstructure and Chemical State,

The surface finish and chemical state of the cathode are important because they determine to a large extent the thermal radiation and electron emission properties of the surface. In the models the radiant heat flux varies directly with the emittance and the current density depends exponentially on the work function. Thorium oxide is added to tungsten during the sintering process, and at high operating temperatures is reduced by the tungsten, forming thorium metal which diffuses

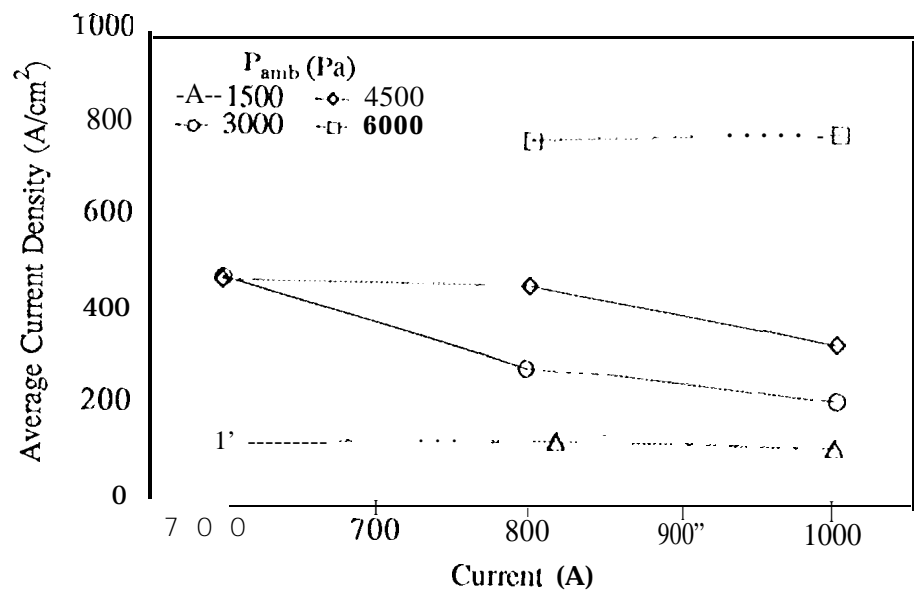


Figure 14: Average current density in the attachment zone.

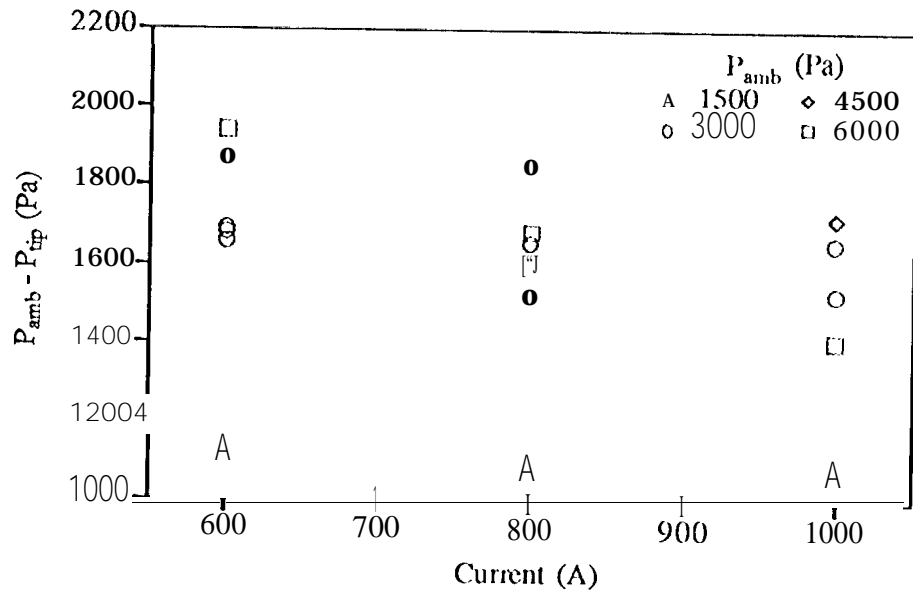


Figure 15: Underpressure observed at the cathode tip.

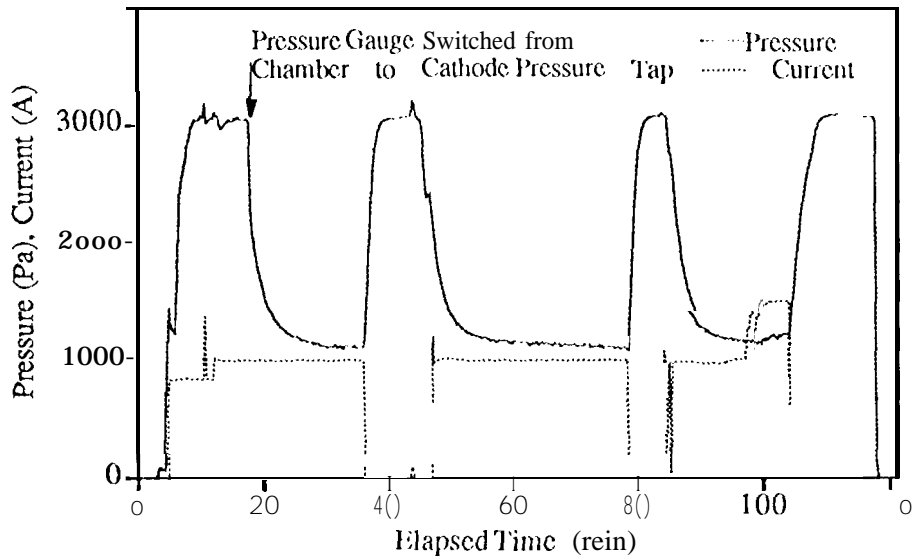


Figure 16: Experiments conducted to test operation of the pressure tap.

to the surface and forms an adsorbate layer. The electric dipole layer formed by this electropositive atom on tungsten lowers the cathode work function, facilitating the escape of electrons from the surface and allowing a lower operating temperature. The variation in the work function with thorium coverage is shown in Fig. (17) [12]. The coverage f is defined by σ/σ_0 , where σ is the surface density of adsorbed thorium atoms and σ_0 represents the number density at the minimum work function. At low coverage the work function approaches that of pure tungsten, about 4.5 eV, while at high coverage the work function is close to that of bulk thorium metal, about 3.27 eV. At high temperatures the thorium metal evaporates from the surface. The equilibrium surface coverage, which determines the lowering of the work function, is dependent on the relative rates of supply by diffusion from the cathode interior and loss by evaporation and mass transport through the surrounding plasma [4]. Because of the extreme model sensitivity to this parameter, it is essential to characterize the extent of thorium coverage on the cathode surface.

In this study five separate examination of cathodes using EDS in an electron microscope were performed. The first cathode had been operated for a total of approximately 20 hrs and the final run had lasted about 1 hr. The same cathode was then polished and examined, and then tested for about 12 sec and studied again. The pressure tap cathode, with a cumulative operating time of 13.3 hrs was examined after a final run of 6.5 min. Finally, the cathode with the cavities was examined after a final runtime of 5 hrs, 13 min and a total operating time of 8 hours.

The examination of the polished cathode showed a pure tungsten surface scored by sandpaper with no appreciable thorium coverage. After the 12 sec run the surface microstructure was dominated by the surface cratering which occurs during the start phase. On start-up, the cathode

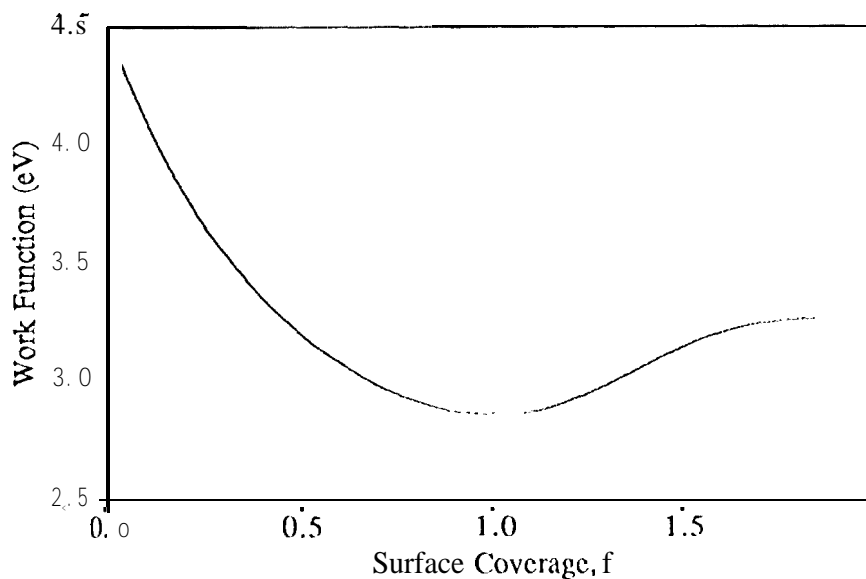


Figure 17: Variation of work function with thorium coverage on tungsten.

surface is too cold to support thermionic emission, so current continuity is maintained by a number of highly mobile hot spots. Although the bulk temperature is low, the local temperature in these emission sites is well above the boiling point of the metal, so vigorous vaporization and "melting" occurs. This extremely destructive process forms small craters with dimensions ranging from less than a micron to several hundred microns. The emission sites heat the cathode, and after several seconds the bulk cathode temperature becomes sufficiently high and the attachment transitions to the thermionic mode discussed above. However, in the process the original surface becomes obliterated by the cratering from thousands of tiny emission sites. The crater size increases with bulk cathode temperature, so the largest craters are formed in the highest temperature region just before transition to the thermionic mode. The SEM examination revealed that a number of these large craters had deposits of thorium in them. Figure (18) is a photomicrograph showing a representative crater with a diameter of about 100 micrometers found on the tip of this cathode. The lighter smooth regions and globules are thorium metal. The cratering process apparently serves to excavate deposits of thorium from the cathode bulk.

The cathode tested for 6 minutes was similar in appearance to the cathode tested for 12 sec. The microstructure on the shaft of the cathode that had been operated for about 1 hr was also dominated by the initial cratering process; however, significant surface restructuring and redistribution of thorium had occurred on the tip. A large circular region on the tip was composed of a porous tungsten structure that looked like a coral reef. This was surrounded by a ring composed of tiny rectangular crystals of pure tungsten, as shown in Fig. (19). Many of the large craters were filled to the rim with porous accumulations of these crystals, as shown in Fig. (20). These structures

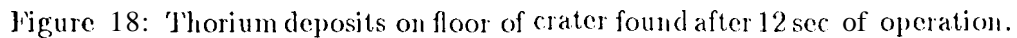


Figure 18: Thorium deposits on floor of crater found after 12 sec of operation.

are probably formed by recrystallization of tungsten at high operating temperatures or by vapor deposition of tungsten.

The most astonishing feature of this cathode, however, was the enormous concentration of thorium on the tip. The rough, ligher material smeared amongst the crystalline structures in Fig. (19) is thorium metal. Such deposits were found all over the tip, demonstrating clearly that some process results in the concentration of thorium on the hottest part of the cathode surface.

Examination of the shaft of the cathode that had been run for over five hours revealed thorium deposits on the floor of large craters about 15 mm from the tip. The shaft downstream of this point appeared to be depleted of thorium. Substantial restructuring of the tip had also occurred on this cathode, with the characteristic tungsten crystals, coral-like structures and clogged craters. However, on the extreme tip was an extraordinary new feature. A circular region approximately 1.6 mm in diameter was composed of structures that looked like fern leaves, as shown in Fig. (21). The stem and ribs of the structures are pure tungsten, and the material that appears to have flowed between them is pure thorium. A magnified image of one of the leaves is shown in Fig. (22). EDS analysis reveals that thorium metal has accumulated between each of the ribs shown in this photomicrograph. In other areas on the tip the surface was composed of scalloped or wave-like structures as shown in Fig. (23). Each of these pure tungsten depressions is filled with a tiny lake of thorium. The cathode tip temperature exceeds the melting temperature of thorium, so the cathode tip must operate with pools of molten thorium metal which collect in the depressions between the tungsten structures.

Thorium can apparently be supplied to the surface from a thin layer by diffusion along grain

Figure 19: Smooth tungsten **crystals** with deposits of thorium found after 1 hour of operation

Figure 20: Craters clogged with tungstencrystals after 1 hour of operation.

Figure 21: Tungsten and thorium structures found on the tip after 5 hours of operation.

Figure 22: Magnified image of the fern-like structures.



Figure 23: Tiny tungsten depressions filled with thorium metal.

boundaries or pores [13], and at the temperatures observed in these experiments the desorption rate of thorium greatly exceeds the diffusion rate from the interior. The discovery of large quantities of thorium on the hottest part of the cathode proves the existence of an additional mass transport step which limits the rate of thorium loss. Zimin has proposed that thorium is ionized in the arc and drawn back to the surface by the electric field near the cathode[14]. This recycling of thorium metal could explain the observed results. The cold cathode cratering process exposes new deposits of thorium during startup. During steady state operation the thorium evaporates rapidly in the tip and further upstream on the shaft. The thorium vapor diffuses into the intense discharge zone near the cathode tip and is ionized and drawn back to the surface. The supply rate by this mechanism is evidently sufficiently high compared to the evaporation rate to result in bulk condensation on the tip. This is a powerful mechanism for the transport of thorium from the cooler parts of the shaft to the hottest region, and it relies completely on the existence of the arc to function. This process results in the depletion of the thorium supply on the shaft, so the work function in this region will increase as the coverage decreases. The tip work function may also increase initially as the coverage passes through the value $f=1$ and forms bulk thorium lakes on the surface. The electron emission on the tip may be dominated by emission from the bulk thorium sites or from thoriated tungsten surfaces between the bulk deposits, so it is difficult to conclude what the effective work function would be from this evidence.

This physical picture may explain the thermal transient behavior observed in the experiments. The initial increase in tip temperature may be associated with the buildup of thorium, after which the effective work function becomes stable at some value between the minimum and that of bulk

thorium. The tip temperature then becomes stable. However, depletion of thorium still occurs along the shaft, requiring increasing temperatures to maintain the emission component from this part of the attachment. This process obviously cannot continue indefinitely. Gradual loss of thorium, even rate-limited by the gas transport processes, will eventually deplete the resources uncovered in the cratering process or available from thin surface layers.

The microstructural changes that occur during operation may also affect the radiant heat flux and the temperature measurements. Surface roughening by formation of the porous structures can increase the surface emittance, while subsequent thermal polishing can cause it to decrease. Further characterization of long-term material behavior is required to resolve this issue.

conclusions

The database of cathode axial temperature profiles has been extended to ambient argon pressures as high as 6000 Pa for current levels ranging from 600 to 1000 A. However, the transient behavior of the temperature distribution complicates comparison with model predictions. The emittance measurements suggest a value ranging from 0.53 to 0.66 is appropriate, probably as a result of surface roughening. Recent comparisons of the models with preliminary temperature measurements agreed well at a current level of 1000 A and below using this emittance, but this appears to produce too much cooling along the cathode shaft for currents above 1000 A. Additional testing is required to extend the measurements further upstream on the shaft. The size of the attachment area was characterized based on argon ion line intensity distributions, yielding trends that agree with model predictions but absolute values that are much higher than those given by the models. The existence of a much smaller luminous plasma region near the cathode tip and a small area of tungsten recrystallization and thorium accumulation on the tip suggests that the most active attachment zone is much smaller than the extent of the plasma luminosity. The pressure tap measurements consistently showed tip pressures substantially lower than the tank pressure measured on the chamber door. Further experiments with additional pressure taps to measure the ambient pressure closer to the attachment zone are planned. The surface examinations revealed that thorium deposits are exposed by the cold cathode cratering process and subsequent segregation of thorium metal occurs over the cathode surface during steady state operation. The thorium is depleted on the cathode shaft and preferentially deposited on the cathode tip, possibly because it is ionized in the plasma near the tip and drawn back to the surface by the electric field. These observations place bounds on the tip work function, but the axial and temporal variations in thorium coverage complicate the models.

Acknowledgements

The research described in this paper was conducted at the Jet Propulsion Laboratory, California Institute of Technology, under a contract with the National Aeronautics and Space Administration.

The authors would like to thank W.J. Thogmartin, R.L. Toomath and A.G. Owens for their technical assistance and dedication in constructing the cathode test facility. The assistance of S. Lewis and M. Cerezo in the JPL Standards Laboratory in calibrating the imaging pyrometer is gratefully acknowledged.

References

- [1] J.E. Polk, A.J. Kelly, and R.G. Jahn. Mechanisms of Hot Cathode Erosion in MPD Thrusters. In 21st *International Electric Propulsion Conference*, Orlando, FL, 1990. AIAA-90-2673.
- [2] K. D. Goodfellow and J. E. Polk. High Current Cathode Thermal Behavior, Part 1: Theory. In 23rd *International Electric Propulsion Conference*, Seattle, WA, 1993. IEPC 93-030.
- [3] K. D. Goodfellow and J. E. Polk. Theoretical Operation of Solid Rod Cathodes. In 30th *Joint Propulsion Conference*, Indianapolis, IN, 1994. AIAA 94-3132.
- [4] J. E. Polk and K. D. Goodfellow. High Current Cathode Thermal Behavior, Part 11: Experiments. In 23rd *International Electric Propulsion Conference*, Seattle, WA, 1993. IEPC 93-029.
- [5] G.N. Hatsopoulos and E.P. Gyftopoulos. *Thermionic Energy Conversion, Vol. II: Theory, Technology, and Application*. MIT Press, Cambridge, MA, 1979.
- [6] R. G. Jahn J. Fillmore, A. J. Kelly. Electric Propulsion laboratory Progress Report. Technical Report MAE 1776.42, Department of Mechanical and Aerospace Engineering, Princeton University, Princeton, NJ 08544, March-April 1993.
- [7] J.C. DeVos. A New Determination of the Emissivity of Tungsten Ribbon. *Physica*, 20:690714, 1954.
- [8] R.M. Myers, N. Suzuki, A.J. Kelly, and R.G. Jahn. Cathode Phenomena in a Low Power, Steady MPD Thruster. In 24th *Joint Propulsion Conference*, Boston, MA, 1988. AIAA-88-3206.
- [9] A. I. Funai and R.E. Rolling. Inspection Techniques for the Characterization of Smooth, Rough, and Oxide Surfaces. In G.B. Heller, editor, *Progress in Aeronautics and Astronautics*. 1967.
- [10] H. Hügel and G. Krüsse. Phänomenologie und Energiebilanz von Lichtbogenkatoden bei niedrigen Drücken und hohen Stromstärken. *Beiträge aus der Plasma Physik*, 9(2):87-11 G, 1969.
- [11] A. C. Malliaris. Phenomena in the Cathode Region of an MPD Accelerator. In *AIAA 5th Aerospace Sciences Meeting*, New York, NY, 1967. AIAA-67-47.
- [12] W.H. Brattain and J.A. Becker. Thermionic and Adsorption Characteristics of Thorium on Tungsten. *Phys. Rev.*, 43:428-450, 1933.
- [13] J. E. Polk. Operation of Thoriated Tungsten Cathodes. In 10th *Symposium, Space Nuclear Power Systems*, Albuquerque, NM, 1993.
- [14] A.M. Zimin, V.I. Khvesyuk, and B.D. Tsypypov. Dynamics of Processes on Activated Cathodes. *Teplofizika Vysokikh Temperatur*, 24(1):30-36, 1986.

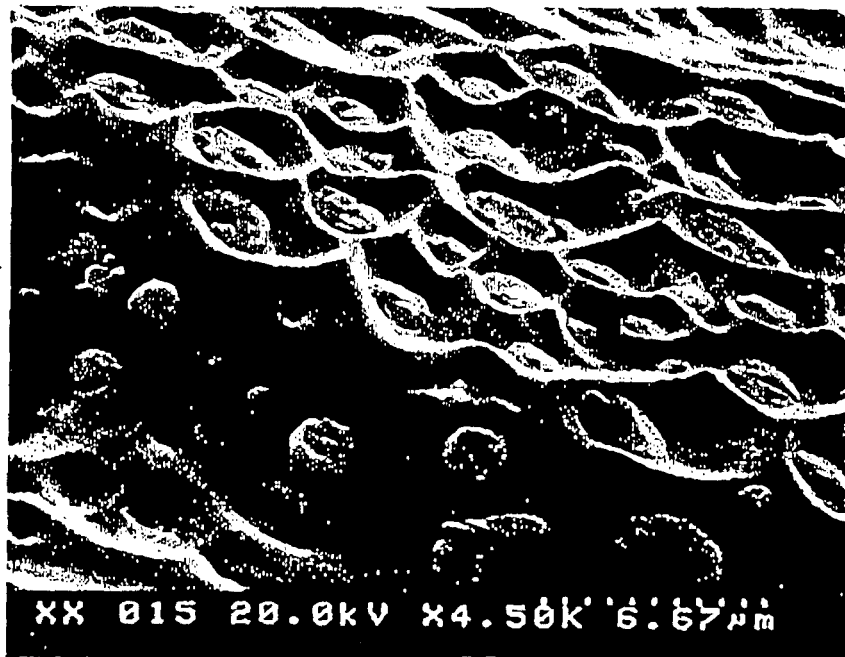


Figure 23: Tiny tungsten depressions filled with thorium metal.

boundaries or pores [13], and at the temperatures observed in these experiments the desorption rate of thorium greatly exceeds the diffusion rate from the interior. The discovery of large quantities of thorium on the hottest part of the cathode proves the existence of an additional mass transport step which limits the rate of thorium loss. Zimin has proposed that thorium is ionized in the arc and drawn back to the surface by the electric field near the cathode [4]. This recycling of thorium metal could explain the observed results. The cold cathode cratering process exposes new deposits of thorium during startup. During steady state operation the thorium evaporates rapidly in the tip and further upstream on the shaft. The thorium vapor diffuses into the intense discharge zone near the cathode tip and is ionized and drawn back to the surface. The supply rate by this mechanism is evidently sufficiently high compared to the evaporation rate to result in bulk condensation on the tip. This is a powerful mechanism for the transport of thorium from the cooler parts of the shaft to the hottest region, and it relies completely on the existence of the arc to function. This process results in the depletion of the thorium supply on the shaft, so the work function in this region will increase as the coverage decreases. The tip work function may also increase initially as the coverage passes through the value $f=1$ and forms bulk thorium lakes on the surface. The electron emission on the tip may be dominated by emission from the bulk thorium sites or from thoriated tungsten surfaces between the bulk deposits, so it is difficult to conclude what the effective work function would be from this evidence.

This physical picture may explain the thermal transient behavior observed in the experiments. The initial increase in tip temperature may be associated with the buildup of thorium, after which the effective work function becomes stable at some value between the minimum and that of bulk

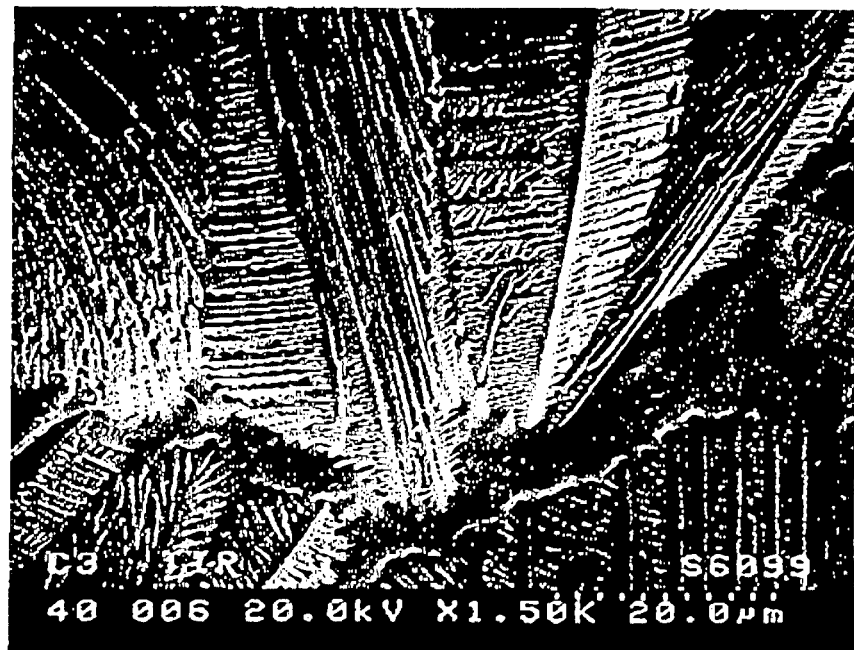


Figure 21: Tungsten and thorium structures found on the tip after 5 hours of operation.

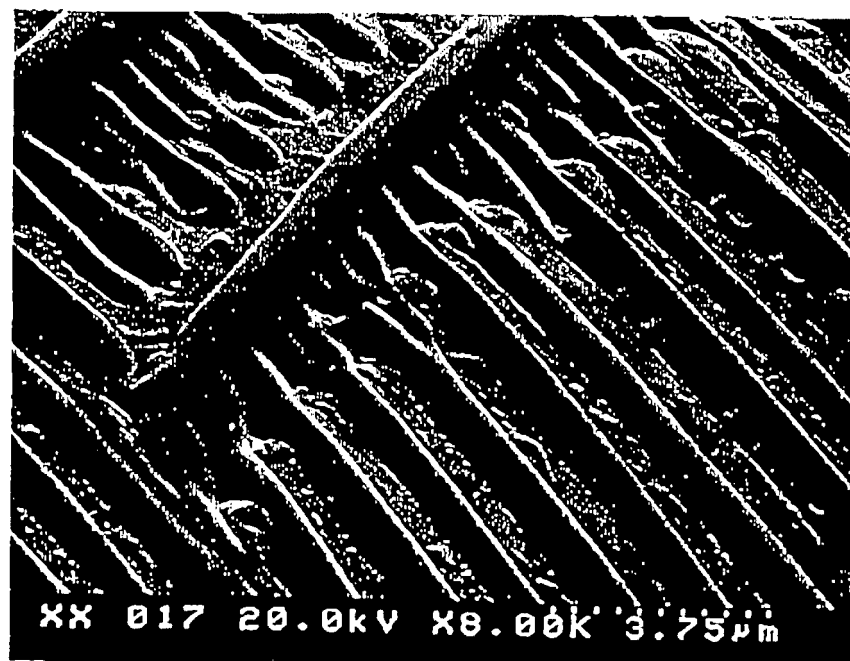


Figure 22: Magnified image of the fern-like structures.

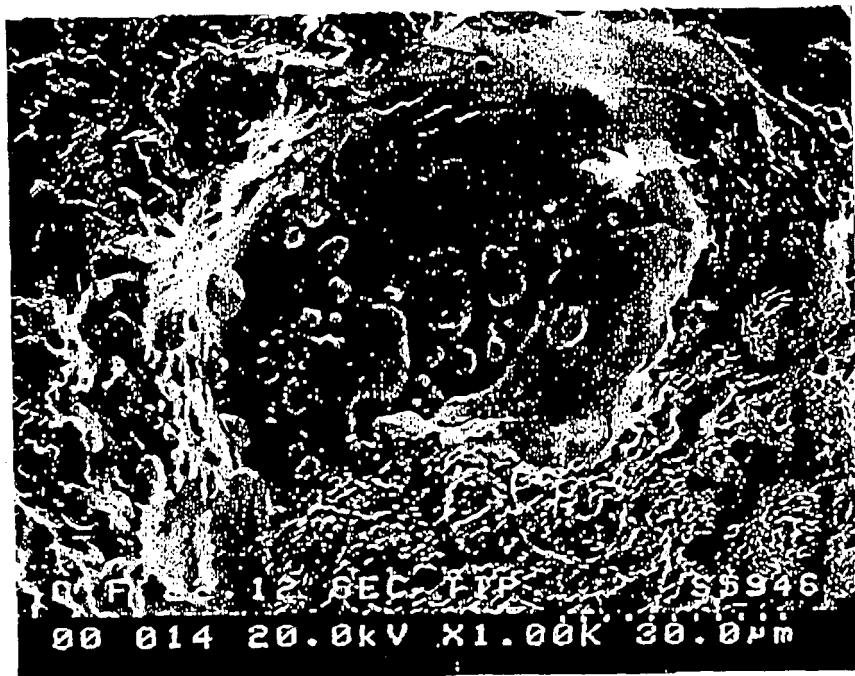


Figure 18: Thorium deposits on floor of crater found after 12 sec of operation.

arc probably formed by recrystallization of tungsten at high operating temperatures or by vapor deposition of tungsten.

The most astonishing feature of this cathode, however, was the enormous concentration of thorium on the tip. The rough, lighter material smeared amongst the crystalline structures in Fig. (19) is thorium metal. Such deposits were found all over the tip, demonstrating clearly that some process results in the concentration of thorium on the hottest part of the cathode surface.

Examination of the shaft of the cathode that had been run for over five hours revealed thorium deposits on the floor of large craters about 15 mm from the tip. The shaft downstream of this point appeared to be depleted of thorium. Substantial restructuring of the tip had also occurred on this cathode, with the characteristic tungsten crystals, coral-like structures and clogged craters. However, on the extreme tip was an extraordinary new feature. A circular region approximately 1.6 mm in diameter was composed of structures that looked like fern leaves, as shown in Fig. (21). The stem and ribs of the structures are pure tungsten, and the material that appears to have flowed between them is pure thorium. A magnified image of one of the leaves is shown in Fig. (22). EDS analysis reveals that thorium metal has accumulated between each of the ribs shown in this photomicrograph. In other areas on the tip the surface was composed of scalloped or wave-like structures as shown in Fig. (23). Each of these pure tungsten depressions is filled with a tiny lake of thorium. The cathode tip temperature exceeds the melting temperature of thorium, so the cathode tip must operate with pools of molten thorium metal which collect in the depressions between the tungsten structures.

Thorium can apparently be supplied to the surface from a thin layer by diffusion along grain

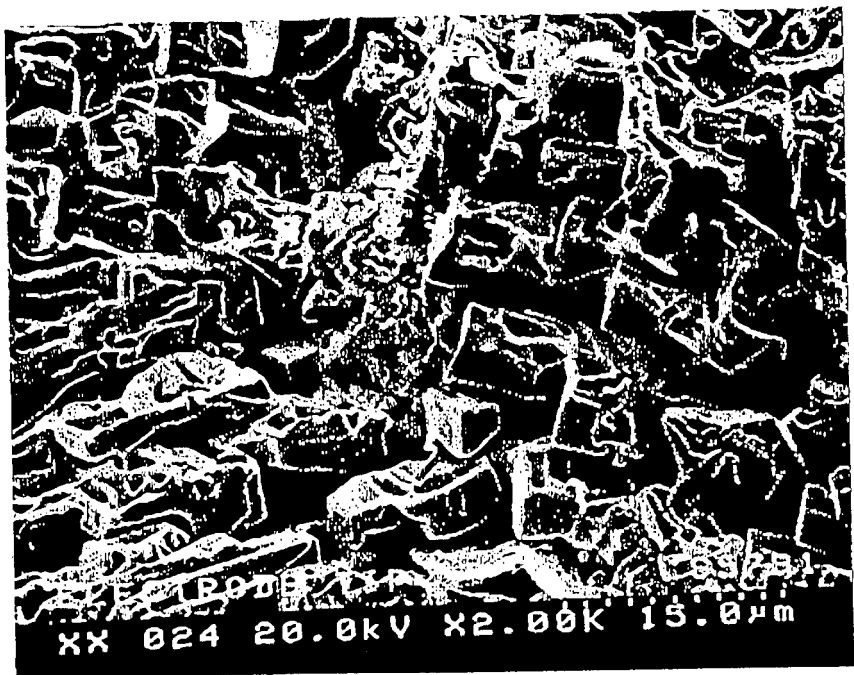


Figure 19: Smooth tungsten crystals with deposits of thorium found after 1 hour of operation.

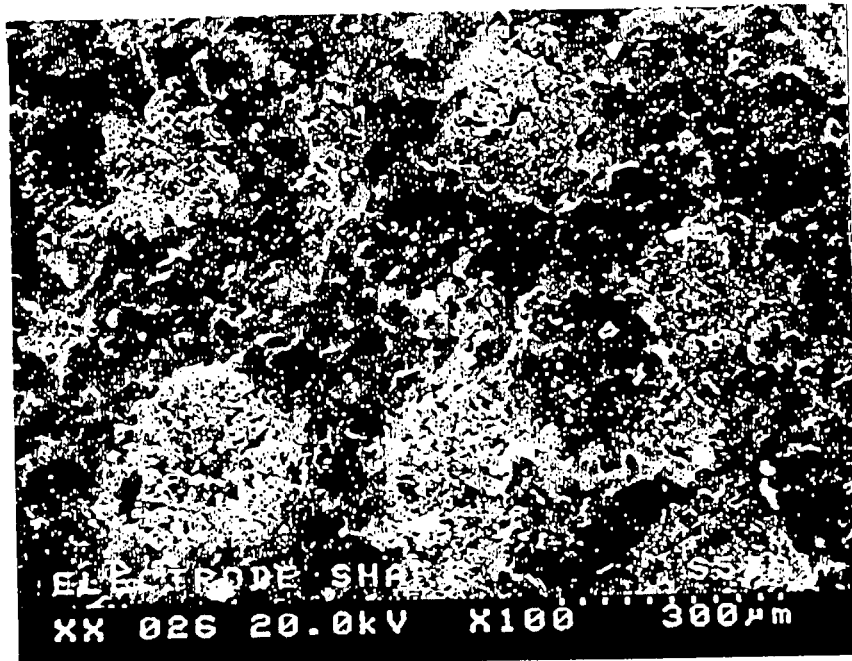


Figure 20: Craters clogged with tungsten crystals after 1 hour of operation.

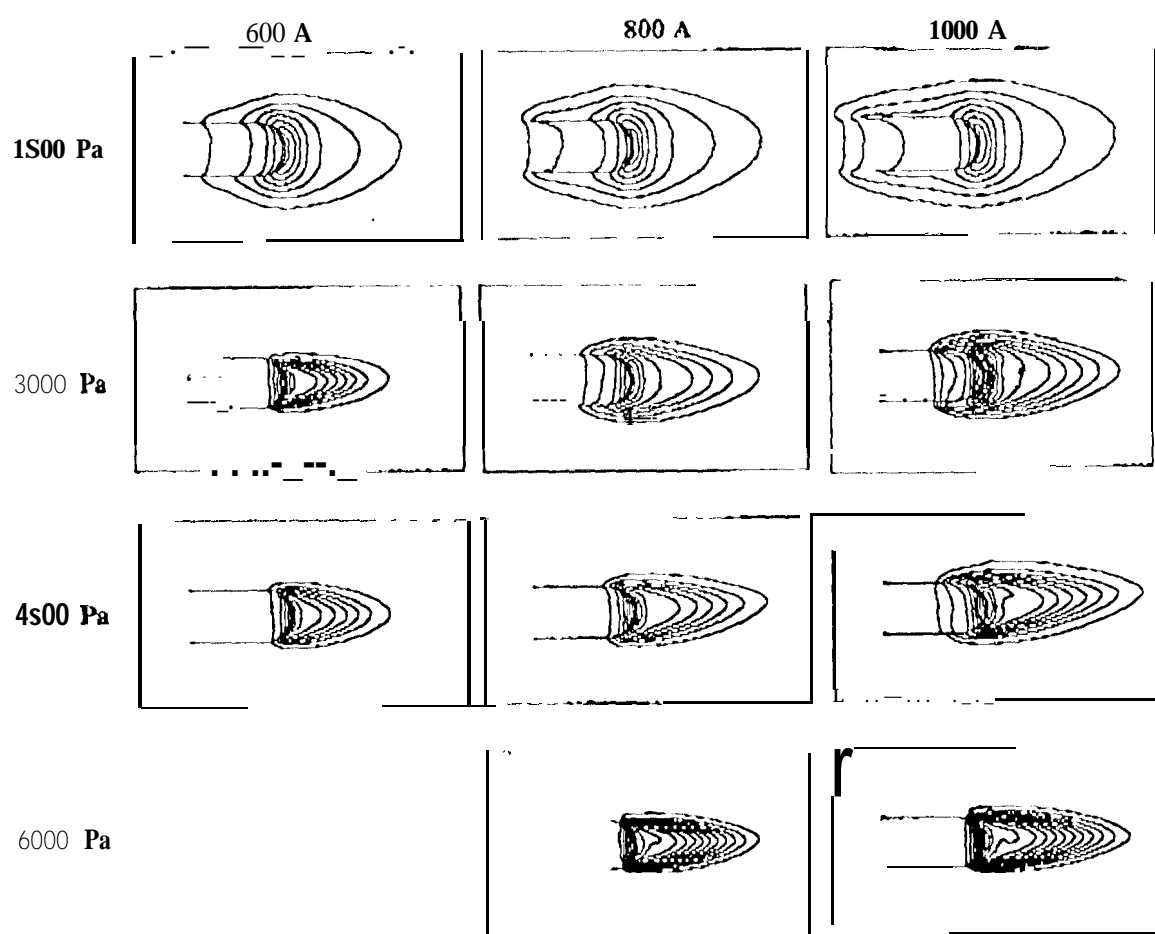


Figure 12: Comparison of 488 nm Ar II line intensity distributions.